Physics of Plasmas

LETTER | FEBRUARY 21 2024

Unveiling non-flat profiles within magnetic islands in tokamaks

Wonjun Tae ; E. S. Yoon ; Min Sup Hur ; G. J. Choi ; J. M. Kwon ; M. J. Choi

Phys. Plasmas 31, 020702 (2024)
https://doi.org/10.1063/5.0179824

Physics of Plasmas LETTER pubs.aip.org/aip/pop

Unveiling non-flat profiles within magnetic islands in tokamaks

Cite as: Phys. Plasmas 31, 020702 (2024); doi: 10.1063/5.0179824
Submitted: 4 October 2023 · Accepted: 24 January 2024 ·
Published Online: 21 February 2024

Wonjun Tae,[1] E. S. Yoon,[1,a)] Min Sup Hur,[1] G. J. Choi,[2] J. M. Kwon,[3] and M. J. Choi[3]

AFFILIATIONS

[1]Ulsan National Institute of Science and Technology, Ulsan 44919, Republic of Korea
[2]Seoul National University, Seoul 08826, Republic of Korea
[3]Korea Institute of Fusion Energy, Daejeon 34133, Republic of Korea

[a)]Author to whom correspondence should be addressed: esyoon@unist.ac.kr

ABSTRACT

The presence of non-flat profiles on magnetic island is studied for the first time through gyrokinetic simulations alongside a simplified Lagrangian model. We have identified that inside a magnetic island, the non-flatness of density and temperature profiles is controlled by a dimensionless parameter $\alpha \equiv w^* \sqrt{\hat{s}\epsilon/q\rho^*}$, which is a function of normalized island width $w^* = w/a_0$, magnetic shear $\hat{s}$, inverse aspect ratio $\epsilon = a_0/R$, safety factor q, and normalized gyroradius $\rho^* = \rho/a_0$. The gyroradius ρ^* dependence of the control parameter α leads to a species-selective transition of profiles from flat to concave only for electrons having high $\alpha \sim \mathcal{O}(1)$. The finding elucidates that electron profiles tend to increasingly deviate from the flat state for a larger magnetic island, in contrast to the conventional wisdom.

In magnetic confinement fusion research, the magnetic island is a phenomenological manifestation of the current perturbation resonating with the rational surface of the nested tori magnetic field configuration in a confined toroidal fusion plasma leading to a magnetic reconnection between the rational surface and neighboring magnetic surfaces originally separated from each other.[1,2] As a consequence, followed strong parallel transport along the reconnected field lines equilibrates radially different plasma distributions. In that regard, plasma density and temperature profile flattenings in the magnetic island have been thought to be a conventional signature of the presence of the magnetic island.

However, in a theoretical sense, profile flattening over the entire inner region of the magnetic island is not the only possible outcome of parallel transport. More generally, profile inside the island is a function of the helical flux surface.[3–5] Indeed, a convex or concave plasma profile at the island center has often been reported from fusion experiments[6,7] and simulations.[8] Furthermore, the emergence of an increasingly pronounced manifestation of non-flat space potential as the island width expands,[9] coupled with the presence of a finite slope in electron temperature[10] within the island, prompts a critical inquiry into the resilience and validity of the prevailing concept of profile flattening in magnetic fusion plasmas.

In this Letter, we prove by a simple Lagrangian model that a plasma tends to have a concave profile in a magnetic island at the most fundamental level and identify the key control parameter $\alpha \equiv w^* \sqrt{\hat{s}\epsilon/q\rho^*}$ that determines the profile shape. The α represents the magnitude of the non-trivial part of the effective potential in the particle Lagrangian, which therefore could affect the plasma distribution at the single particle level. Here, $w^* = w/a_0$ is the normalized island width, $\hat{s}$ is the magnetic shear, $\epsilon = a_0/R$ is the inverse aspect ratio, q is the safety factor, and $\rho^* = \rho/a_0$ is the normalized gyroradius, where a_0 and R are minor and major radii, respectively. We then verify via extensive global nonlinear gyrokinetic simulations that our fundamental argument based on the single particle property is robust in realistic tokamak plasmas with collisional and turbulent transport.

Our work reveals several interesting features as follows. First, the gyroradius ρ^* dependence of the control parameter α results in a species-selective profile deviation from the flat state in the island. That is, electrons with high α have concave profiles, while ions with very low α have flat profiles. This indicates an interesting mechanism of vortex flow generation near the island center by profile-induced polarization. Second, the proportionality of α to the island size w leads to a more significant deviation of the profiles from the flat state for a larger island. This is in contrast to the conventional wisdom that a large enough magnetic island has flattened profiles.[11]

To find the control parameters of the profile flattening, we begin with a sheared slab model[12] for the background magnetic field $\overrightarrow{B_0}$ in Cartesian coordinates (x, y, z) as

$$\overrightarrow{B_0} = B_0\left(\hat{z} + \frac{x}{L_s}\hat{y}\right), \tag{1}$$

which can be realized with the following vector potential:

$$\overrightarrow{A_0} = B_0 x\left(\hat{y} - \frac{x}{2L_s}\hat{z}\right), \tag{2}$$

where L_s is the magnetic shear-scale length. The magnetic island perturbation we applied in this model is

$$\overrightarrow{\delta A} = \overline{\delta A}\cos\left(\frac{\pi}{h}y\right)\hat{z}, \tag{3}$$

where we use constant $\overline{\delta A}$ approximation,[1] and h is the island half height. Then, Lagrangian $\mathcal{L}$ in the sheared slab model can be explicitly written as

$$\mathcal{L}(t,x,\dot{x}) = \frac{1}{2}m_a(\dot{x}^2+\dot{y}^2+\dot{z}^2) + q_a\dot{y}B_0x + q_a\dot{z}\left\{-B_0\frac{x^2}{2L_s} + \overline{\delta A}\cos\left(\frac{\pi}{h}y\right)\right\}, \tag{4}$$

where m_a and q_a are the mass and charge for species a, respectively. In this model, we assume a negligible effect of the self-consistent electric field for simplicity. We obtain the corresponding Euler–Lagrange equations for the given Lagrangian as

$$\frac{d}{dt}m_a\dot{x} = \dot{y}q_aB_0 - \dot{z}q_aB_0\frac{x}{L_s}, \tag{5}$$

$$\frac{d}{dt}m_a\dot{y} = -\dot{x}q_aB_0 - \dot{z}q_a\overline{\delta A}\frac{\pi}{h}\sin\left(\frac{\pi}{h}y\right), \tag{6}$$

$$\frac{d}{dt}p_{az} \equiv \frac{d}{dt}\left[m_a\dot{z} + q_a\left\{-B_0\frac{x^2}{2L_s} + \overline{\delta A}\cos\left(\frac{\pi}{h}y\right)\right\}\right] = 0. \tag{7}$$

Note that z is an ignorable coordinate as designed, and its conjugate momenta p_{az} is constant. Also, the curly bracket in the definition of p_{az} corresponds to a conventional flux surface coordinate of magnetic islands.[13,14]

Using Eqs. (5)–(7), energy conservation can be straightforwardly proven by

$$\frac{d}{dt}E_a = 0,$$

where the conserved energy E_a is

$$\text{Const.} = E_a = \frac{1}{2}m_a(\dot{x}^2+\dot{y}^2+\dot{z}^2) \equiv \frac{1}{2}m_a(\dot{x}^2+\dot{y}^2) + \chi_a(x,y),$$

and we define our two-dimensional (2D) effective potential $\chi_a(x,y)$ as

$$\chi_a(x,y) \equiv \frac{1}{2m_a}\left\{p_{az} + \frac{q_aB_0}{2L_s}x^2 - q_a\overline{\delta A}\cos\left(\frac{\pi}{h}y\right)\right\}^2 = \frac{m_a}{2}v_{Ta}^2\left[\frac{p_{az}}{m_av_{Ta}} \pm \frac{1}{2}\left(\frac{w/2}{\sqrt{\rho_{Ta}L_s}}\right)^2 \times \left\{\left(\frac{x}{w/2}\right)^2 - \frac{1}{2}\cos\left(\frac{\pi}{h}y\right)\right\}\right]^2,$$

with island full width

$$w = 4\sqrt{\frac{L_s\overline{\delta A}}{B_0}}.$$

Here, the plus sign is for ions and the minus sign is for electrons. Note that the effective potential induced by the perturbed magnetic field becomes prominent when the geometric mean of the gyroradius and magnetic field scale are comparable to or less than the island half width. Figure 1 plots the effective potential. Considering $L_s \sim qR/\hat{s}$ in the sheared slab approximation of the toroidal plasmas and the usual parameter range of concern including $w = 10$–$60\ \rho_i$,[15] the characteristic order for electrons,

$$\frac{w/2}{\sqrt{\rho_{Te}L_s}} \gtrsim O(1),$$

indicates that electron motions can be significantly affected by the presence of the effective potential. We note that the effect of this factor can be more pronounced for electrons than ions due to their small gyroradius. The origin of this effective potential shares similarities with the drift motions and energetics in magnetic mirrors, i.e., conservation of canonical momentum in the z direction due to symmetry, Eq. (7), in conjunction with the energy conservation limits manifold of particle's presence in the configuration space. We would like to emphasize that this process is related to not arbitrary projection of physics quantities or coordinate transformation but the constraint imposition. Substituting the approximate description of the local magnetic shear for toroidal geometry $L_s \sim qR/\hat{s}$, the above control parameter can be interpreted for species a as

$$\frac{w/2}{\sqrt{\rho_{Ta}L_s}} \simeq w^*\sqrt{\frac{\hat{s}\epsilon}{q\rho_a^*}} \equiv \alpha. \tag{8}$$

As a result, we can identify four parameters that have an impact on the profile shape of the magnetic island for the given $q = q_0 = m/n$: ratio of island width to minor radius $w^* \equiv w/a_0$, magnetic shear $\hat{s} \equiv (a_0/q)(dq/dr)|_{r(q_0)}$, the inverse aspect ratio $\epsilon \equiv a_0/R$, and ratio of gyroradius to minor radius $\rho^* \equiv \rho/a_0$.

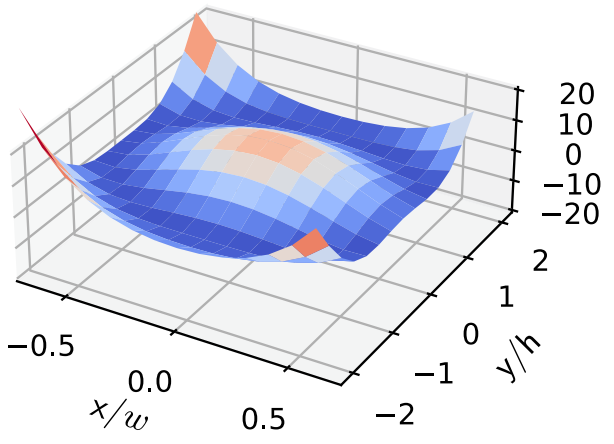

FIG. 1. Effective potential of electrons, $\chi_e(x,y)$ for $p_{az} = 0$, $\rho_e = 2.66 \times 10^{-5}$ m, $w = 0.0798$ m, $L_s = 4$ m and $h = 1$. x and y are radial and binormal coordinates, and O- and X-points correspond to $(x,y) = (0,0)$ and $(0,\pm 2)$, respectively.

With the analytic implication of the above findings, we investigated the parameter dependency from the effective potential model using the gyrokinetic code GENE (Gyrokinetic Electromagnetic Numerical Experiment).[16] GENE is a continuum code that solves nonlinear gyrokinetic Vlasov–Maxwell equations self-consistently in five-dimensional (5D) phase space with straight field coordinates including radial (x) coordinate.[17]

The simulation results below are from the parameter setup as follows. Electrostatic nonlinear global simulation is conducted to fix the magnetic island but includes the self-consistent electric field effect so that we can see the impact of induced electric potential as well as the effective magnetic field potential. A relatively large electron-to-ion mass ratio of 1:400 is used to reduce computational cost; its consequence does not show much difference with cases using the genuine mass ratio. Concentric circular magnetic field geometry[18] is used by setting plasma beta $\beta = 0$ in the electrostatic limit. The center of both the magnetic island and the simulation domain is at $x_0 = 0.5a_0$ where safety factor $q = q_0 = m/n = 2/1$ is located, and correspondingly, the aspect ratio at magnetic island center $\epsilon_I = x_0/R = a_0/2R = \epsilon/2$ ranges 0.06–0.3 for the fixed relative position of the island to the minor radius. The linearized Fokker–Plank operator is used for collision, and collisionality in simulation is set to 0.003 ($=0.236\,\nu_e^*$) in the banana regime. $k_{y,\min}\rho_i = 0.01$ is used to sufficiently cover fluctuations around magnetic islands. The default grid size is set to $\{x \times y \times z \times v \times w\} = 256 \times 64 \times 16 \times 32 \times 8$ for all simulations unless change is stated below. To clearly separate the effect of each parameter in α, we carefully fix all the other variables to scan one varying parameter considering island width is a function of magnetic shear and geometric parameters are related to each other.

One-dimensional (1D) electron density and temperature profiles radially across the O-point of the magnetic island for low and high α cases are compared in Fig. 2. Initial profile is designed to have a gradient profile $\kappa_s \cosh\{(x - x_0)/L_c\}$ such that the peak of the gradient κ_s is located at the profile center x_0. We set $\kappa_n = 2.2$ and $\kappa_T = 3$ for both species. In the absence of island field perturbation with the initial profile, ion temperature gradient (ITG) turbulence is sufficiently weak to isolate flattening physics from turbulence-spreading phenomena.[19] The island width 10–50 ρ_i is scanned, and all profiles are measured at the $z = 0$ midplane radially crossing the O-point of the island.

To quantify the extent of profile distortion from flat state, we introduce the measure g_Λ,

$$g_\Lambda \equiv \frac{\Lambda\left(x_0 - \frac{w}{2}\right) + \Lambda\left(x_0 + \frac{w}{2}\right)}{2} - \min_{\left[x_0 - \frac{w}{2}, x_0 + \frac{w}{2}\right]} \Lambda(x),$$

which is the difference of the physical quantity $\Lambda \in \{n, T\}$ between the average of the values at two boundaries of the island and the lowest profile value within the island region. In Figs. 2(a) and 2(b), the distortion measure for low α indicates a flattening of the profiles as in usual cases of magnetic islands. Such flattening is visible for both ion and electron temperature and electron density. In this case, g is almost zero. However, no profile flattening occurs in the electron density and temperature profiles when α is high. In the high α case, the profile becomes concave, and g has a higher value. From the perspective of the previously shown effective potential structure in Fig. 1, the collapses of electron density and temperature at the island center in this case are attributed to the unavailable access and the reduced kinetic energy by the high effective potential, respectively. Also, the profile closely follows the flux function of the magnetic island, much like the effective potential. In addition to the consideration of the effective potential discussed herein, there is a report[20] in flux-driven fluid simulations attributing non-flat profiles to turbulence penetration. However, the ion temperature profile for high α is similar to that of low α in Fig. 2(c), which can be attributed to the comparatively insensitive dependence on the effective potential of ions.

To confirm the effectiveness α in the effective potential as a control parameter of the profile flattening, we conduct parameter scan of the distortion g for each factor of the α, i.e., w, $\hat{s}$, ϵ_I, and ρ^* as shown in Fig. 3. In Fig. 3(a), g_{ne} increases with $\hat{s}$, $1/\rho^*$, and ϵ_I, respectively, at $w^* = 1/8$ as expected from Eq. (8) showing the relation based on the effective potential model. It has been reported that the excitation of NTM varies with the critical beta changes due to the ρ^* scaling.[21] Figure 3(b) shows deviation g for the electron density profile as a function of ϵ and magnetic island width. For the fixed ratio of island position to plasma minor radius $x_0/a = 0.5$, we used $\epsilon_I = r/R_0$ instead of ϵ as the scanning parameter in our simulations. It is shown that the higher ϵ_I is, the greater g is. The magnetic island width has the same trend as ϵ_I. We note that Fig. 3(b) reveals that the small island width case does not show the concave profile, even with a high ϵ_I. From the perspective of the critical width, where temperature becomes a function of island flux surface,[11] a width of 10 ρ_i appears to be lower than the critical width (critical width ~15–20 ρ_i, with $\chi_\perp/\chi_\parallel \sim 10^{-6}$). Breakdown of scaling at small $\hat{s}$ and $1/\rho^*$ is also notable.

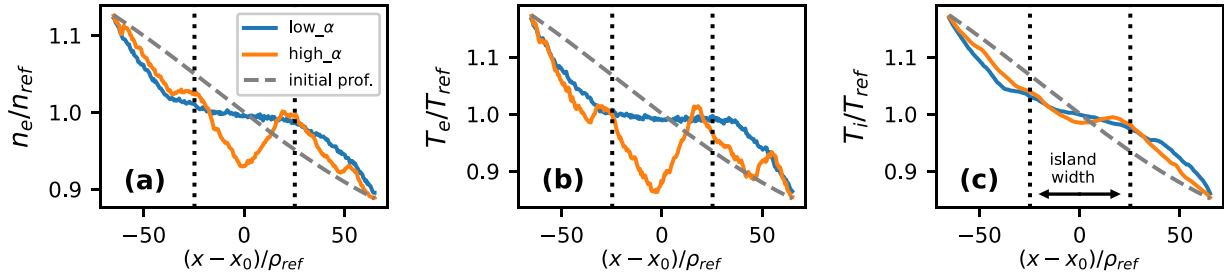

FIG. 2. Profile comparing low and high α magnetic island cases at the O-point of the $z = 0$ plane for (a) electron density, (b) electron temperature, and (c) ion temperature. The low α (=0.433) case shows conventional profile flattening in electron density, electron temperature, and ion temperature. The high α (=0.75) case shows a concave profile in the magnetic island region in electron density and electron temperature, while ion temperature still shows profile flattening.

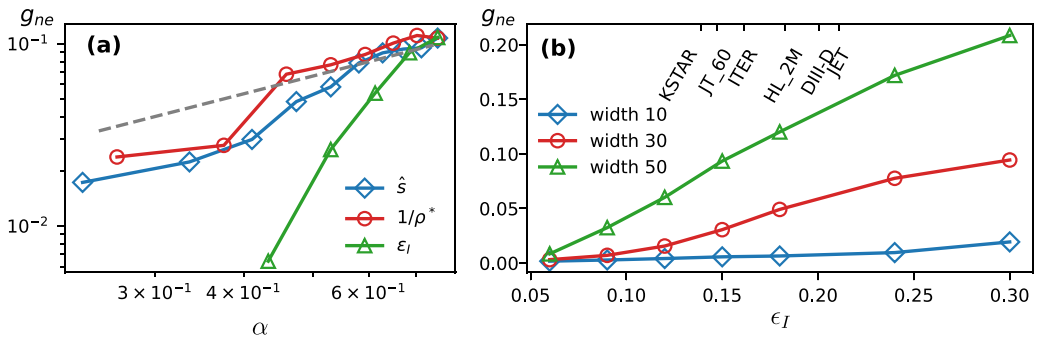

FIG. 3. Parameter scans of profile deviation g_{ne} (a) for $\hat{s}$, $1/\rho^*$ and ϵ_I over α in a log–log plot and (b) over ϵ_I and island width (in ρ_i unit). The half of inverse aspect ratio $\epsilon = a_0/2R_0$ for experimental devices is denoted for relevance. Trends of parameter dependence for all variables are consistent with the effective potential model.

Figure 4 shows 2D plots of perturbed electron density deviation from initial profiles for low and high α case magnetic islands by different ϵ_I values at the $z=0$ midplane. For low α, Fig. 4(a) shows negative (positive) profile deviation on the left (right) of the island center. Considering the initial gradient of the background profiles, such deviation implies a flattening of the profiles by strong parallel transport along the reconnected field lines. For high α, on the other hand, a new structure breaking the flattened profiles near the center of the island is found, as shown in Fig. 4(b). Electron density fluctuation has a more complex structure, with a dominant negative deviation at the center of the magnetic island. This hollowed-out island center corresponds to the shape of the effective potential. Figure 4(c) exhibits the total density of Fig. 4(b). A strong correlation between the effective potential and the structure around the *O*-point can be clearly observed by comparison between Figs. 1 and 4(c).

In conclusion, we investigate the role of magnetic perturbation as an effective potential in the profile flattening inside a magnetic island. The simplified Lagrangian model in sheared slab geometry reveals that the effective potential by the magnetic island perturbation, characterized by the key control parameter $\alpha = w^*\sqrt{\hat{s}\epsilon/q\rho^*}$, can be remarkably pronounced with increasing island size w^*, magnetic shear $\hat{s}$, inverse aspect ratio ϵ, and inverse gyroradius $1/\rho^*$. The close relation between the profile flattening and the analytically predicted parameter dependence of the effective potential has been verified through global nonlinear gyrokinetic simulations. In particular, our analytic model predicts that the convex shape of the effective potential with an inverse gradient inside the island leads to concave plasma profiles, and its significance is proportional to α. A gyrokinetic simulation has yielded concave profiles for electrons while flattened profiles for ions in a reference tokamak plasma, consistent with the analytic prediction since $\alpha \sim 1$ for electrons while $\alpha \ll 1$ for ions in this representative example. Controlled simulations with low and high α have shown a clear correlation between the concaveness of the electron profiles and the level of α, demonstrating that our fundamental argument works in realistic fusion plasmas. Results of further systematic scans in $\hat{s}$, $1/\rho^*$, ϵ, and w^* consisting of α support our finding. The result for w^* scan is especially interesting as it indicates that a larger magnetic island is more likely to have finite gradient profiles in contrast to the conventional wisdom that profiles in larger islands get more flattened. We note that the non-flatness structure within the island elucidated in this study differs from the phenomenon of flattening typically discussed with the background profiles.[22] Unfortunately, there have been limited reports in experiments so far that observed concave profiles. We presume that this would be related to the observable island width and resolution of the diagnostics. In order to diagnose the concave structure, precise control over experimental parameters is crucial for systematically exploring the range of α values. Also, we note that a competing effect producing a convex profile by the spontaneous heating process

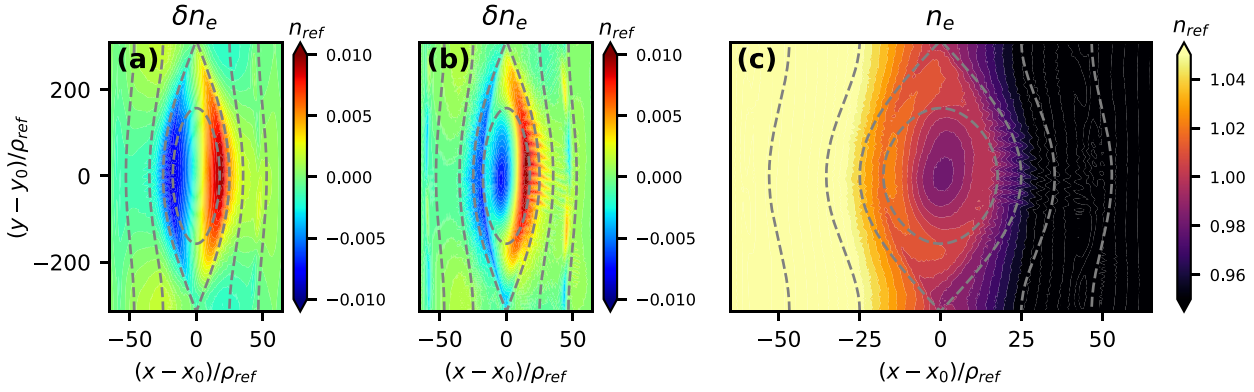

FIG. 4. Perturbed quantities from initial values at the $z=0$ midplane in (x, y) coordinates. (a) Perturbed electron density in the low α case, (b) perturbed electron density, and (c) total electron density in the high α case. The hollowed-out structure of the island center is similar to the shape of the effective potential.

of magnetic island itself is recently reported.[23] The proportionality of α to the inverse aspect ratio ϵ indicates that the concave electron profiles would be more pronounced in a spherical torus (ST) compared to a conventional tokamak.

In recent theories,[14,24–26] simulations[27–29] and experimental investigations,[30–33] active roles of the $E \times B$ vortex flows in magnetic island dynamics have been uncovered. It should be emphasized that we have found concave electron density and flattened ion gyrocenter density profiles inside the island due to different impacts of the effective potential. This indicates that there could be a significant vortex flow formation via profile-induced polarization density[34,35] in the central region of the island, which is a different mechanism from previously studied turbulence-induced vortex flow generation.[24,25]

Furthermore, the identified control parameters for the two-dimensional structure within magnetic islands in this study can offer a novel avenue for refining models that traditionally expect or consider flat profiles, such as those addressing the well-recognized parallel vs perpendicular heat transport balance[11] and turbulence spreading into the magnetic island,[36,37] leading to more sophisticated and accurate models. Future investigations will focus on the experimental observation of convexity, the analytic exploration of self-consistent electric field effects on the island profile flattening, the electromagnetic effect on the non-flatness of magnetic island, and the effect of the non-flatness on magnetic fusion confinement. Also, the effect of the distorted profiles on the island width dynamics with regard to the bootstrap[38] and polarization current can be further explored.

The authors acknowledge useful discussions with Professor T. S. Hahm and referees. This work was supported by a National Research Foundation of Korea grant funded by the Korean Government (No. NRF-2019M1A7A1A03088462). Also, this research was supported by the R&D Program through the Korea Institute of Fusion Energy (KFE) funded by government of the Republic of Korea (No. KFE-EN2341) and the Korea Institute of Energy Technology Evaluation and Planning and the Ministry of Trade, Industry & Energy (MOTIE) of the Republic of Korea (Grant No. 20214000000410). Computing resources were provided on the KFE computer KAIROS, funded by the Ministry of Science and ICT of the Republic of Korea (No. KFE-EN2341-9), and supported by the National Supercomputing Center with supercomputing resources including technical support (No. KSC-2022-CRE-0392).

AUTHOR DECLARATIONS

Conflict of Interest

The authors have no conflicts to disclose.

Author Contributions

Wonjun Tae: Conceptualization (lead); Data curation (lead); Formal analysis (equal); Investigation (lead); Methodology (lead); Visualization (lead); Writing – original draft (lead); Writing – review & editing (lead). **E. S. Yoon:** Conceptualization (equal); Formal analysis (equal); Funding acquisition (lead); Methodology (equal); Resources (lead); Supervision (lead); Writing – original draft (equal); Writing – review & editing (equal). **Min Sup Hur:** Funding acquisition (equal); Project administration (equal); Resources (equal); Supervision (equal). **G. J. Choi:** Formal analysis (equal); Investigation (supporting); Methodology (supporting); Supervision (supporting); Writing – review & editing (equal). **J. M. Kwon:** Funding acquisition (supporting); Project administration (lead); Resources (equal); Supervision (supporting). **M. J. Choi:** Formal analysis (equal); Investigation (supporting); Project administration (supporting); Supervision (supporting); Writing – review & editing (equal).

DATA AVAILABILITY

The data that support the findings of this study are available within the article.

REFERENCES

[1]H. P. Furth, J. Killeen, and M. N. Rosenbluth, Phys. Fluids **6**, 459 (1963).
[2]H. Zohm, *Magnetohydrodynamic Stability of Tokamaks* (Wiley-VCH, 2015).
[3]R. D. Hazeltine and J. D. Meiss, *Plasma Confinement* (Dover Publications, New York, 2003).
[4]M. J. Choi, G. S. Yun, W. Lee, H. K. Park, Y.-S. Park, S. A. Sabbagh, K. J. Gibson, C. Bowman, C. W. Domier, N. C. Luhmann, Jr. *et al.*, Nucl. Fusion **54**, 083010 (2014).
[5]L. Bardóczi, T. L. Rhodes, T. A. Carter, R. J. L. Haye, A. B. Navarro, and G. R. McKee, Phys. Plasmas **24**, 062503 (2017).
[6]C. Yu, D. L. Brower, S. Zhao, R. V. Bravenec, J. Chen, H. Lin, Jr., N. C. Luhmann, W. A. Peebles, C. P. Ritz, P. M. Schoch, and X. Yang, Nucl. Fusion **32**, 1545 (1992).
[7]P. C. de Vries, G. Waidmann, A. Kramer-Flecken, A. J. H. Donne, and F. C. Schuller, Plasma Phys. Controlled Fusion **39**, 439 (1997).
[8]O. Izacard, C. Holland, S. D. James, and D. P. Brennan, Phys. Plasmas **23**, 022304 (2016).
[9]K. Ida, S. Inagaki, N. Tamura, T. Morisaki, N. Ohyabu, K. Khlopenkov, S. Sudo, K. Watanabe, M. Yokoyama, T. Shimozuma *et al.*, Nucl. Fusion **44**, 290 (2004).
[10]X. Tang, Z. Lin, W. W. Heidbrink, J. Bao, C. Xiao, Z. Li, J. Li, and L. Bardóczi, Phys. Plasmas **27**, 032508 (2020).
[11]R. Fitzpatrick, Phys. Plasmas **2**, 825 (1995).
[12]P. H. Rutherford, Phys. Fluids **16**, 1903 (1973).
[13]H. R. Wilson, J. W. Connor, R. J. Hastie, and C. C. Hegna, Phys. Plasmas **3**, 248 (1996).
[14]T. S. Hahm, Y. J. Kim, P. H. Diamond, and G. J. Choi, Phys. Plasmas **28**, 022302 (2021).
[15]A. B. Navarro, L. Bardóczi, T. A. Carter, F. Jenko, and T. L. Rhodes, Plasma Phys. Controlled Fusion **59**, 034004 (2017).
[16]F. Jenko, W. Dorland, M. Kotschenreuther, and B. N. Rogers, Phys. Plasmas **7**, 1904 (2000).
[17]P. Xanthopoulos, D. Mikkelsen, F. Jenko, W. Dorland, and O. Kalentev, Phys. Plasmas **15**, 122108 (2008).
[18]X. Lapillonne, S. Brunner, T. Dannert, S. Jolliet, A. Marinoni, L. Villard, T. Görler, F. Jenko, and F. Merz, Phys. Plasmas **16**, 032308 (2009).
[19]J.-M. Kwon, S. Ku, M. J. Choi, C. S. Chang, R. Hager, E. S. Yoon, H. H. Lee, and H. S. Kim, Phys. Plasmas **25**, 052506 (2018).
[20]A. Ishizawa, Y. Kishimoto, and Y. Nakamura, Plasma Phys. Controlled Fusion **61**, 054006 (2019).
[21]R. J. L. Haye, R. J. Buttery, S. Guenter, G. T. A. Huysmans, M. Maraschek, and H. R. Wilson, Phys. Plasmas **7**, 3349 (2000).
[22]K. Imada, H. R. Wilson, J. W. Connor, A. V. Dudkovskaia, and P. Hill, Nucl. Fusion **59**, 046016 (2019).
[23]D. Villa, N. Dubuit, O. Agullo, A. Poye, X. Garbet, and A. Smolyakov, J. Plasma Phys. **88**(6), 905880613 (2022).
[24]G. J. Choi and T. S. Hahm, Phys. Rev. Lett. **128**, 225001 (2022).
[25]M. Leconte and Y. W. Cho, Nucl. Fusion **63**, 034002 (2023).
[26]G. J. Choi, Nucl. Fusion **63**, 066032 (2023).
[27]K. S. Fang and Z. Lin, Phys. Plasmas **26**, 052510 (2019).
[28]M. Muto, K. Imadera, and Y. Kishimoto, Phys. Plasmas **29**, 052503 (2022).

[29]J. Li, J. Q. Xu, Y. R. Qu, Z. Lin, J. Q. Dong, X. D. Peng, and J. Q. Li, Nucl. Fusion **63**, 096005 (2023).
[30]K. Ida, N. Ohyabu, T. Morisaki, Y. Nagayama, S. Inagaki, K. Itoh, Y. Liang, K. Narihara, A. Yu. Kostrioukov, B. J. Peterson *et al.*, Phys. Rev. Lett. **88**, 015002 (2001).
[31]T. Estrada, E. Ascasíbar, E. Blanco, A. Cappa, C. Hidalgo, K. Ida, A. López-Fraguas, and B. Ph. van Milligen, Nucl. Fusion **56**, 026011 (2016).
[32]T. Estrada, E. Maragkoudakis, D. Carralero, T. Windisch, J. L. Velasco, C. Killer, T. Andreeva, J. Geiger, A. Dinklage, A. Krämer-Flecken *et al.*, Nucl. Fusion **61**, 096011 (2021).
[33]M. J. Choi, Rev. Mod. Plasma Phys. **5**, 9 (2021).
[34]A. J. Brizard and T. S. Hahm, Rev. Mod. Phys. **79**, 421 (2007).
[35]L. Wang and T. S. Hahm, Phys. Plasmas **16**, 062309 (2009).
[36]K. Ida, T. Kobayashi, M. Ono, T. E. Evans, G. R. McKee, and M. E. Austin, Phys. Rev. Lett. **120**, 245001 (2018).
[37]K. Ida, Adv. Phys. **5**, 1801354 (2020).
[38]W. A. Hornsby, M. Siccinio, A. G. Peeters, E. Poli, A. P. Snodin, F. J. Casson, Y. Camenen, and G. Szepesi, Plasma Phys. Controlled Fusion **53**, 054008 (2011).